Proceedings of the ASME 2014 International Mechanical Engineering Congress & Exposition
IMECE 2014
November 14-20, 2014, Montreal, Canada

IMECE2014-40221

STABILITY DETERMINATION IN TURNING USING PERSISTENT HOMOLOGY AND TIME SERIES ANALYSIS

Firas A. Khasawneh *
Mechanical Engineering
State University of New York Institute of Technology
Utica, NY 13502
firas.khasawneh@sunyit.edu

Elizabeth Munch
Institute for Mathematics and its Applications
University of Minnesota
Minneapolis, Minnesota 55455
liz@ima.umn.edu

ABSTRACT

This paper describes a new approach for ascertaining the stability of autonomous stochastic delay equations in their parameter space by examining their time series using topological data analysis. We use a nonlinear model that describes the tool oscillations due to self-excited vibrations in turning. The time series is generated using Euler-Maruyama method and then is turned into a point cloud in a high dimensional Euclidean space using the delay embedding. The point cloud can then be analyzed using persistent homology. Specifically, in the deterministic case, the system has a stable fixed point while the loss of stability is associated with Hopf bifurcation whereby a limit cycle branches from the fixed point. Since periodicity in the signal translates into circularity in the point cloud, the persistence diagram associated to the periodic time series will have a high persistence point. This can be used to determine a threshold criteria that can automatically classify the system behavior based on its time series. The results of this study show that the described approach can be used for analyzing datasets of delay dynamical systems generated both from numerical simulation and experimental data.

INTRODUCTION

Deterministic models for chatter in machining dynamics have been the subject of extensive research in recent years [1]. However, machining processes are inherently stochastic with many noise sources due, for example, to the variation of the material parameters [2,3], external noise sources [4], and variations of the delay [5]. However, the lack of analysis tools for stochastic delay systems remains a fundamental impediment to the continuous progress in the metal removal industry.

Stochastic equations are infinite dimensional and therefore analysis tools from deterministic models are not readily applicable to them. The analysis is more challenging if the dynamics involve delays and the system model is a stochastic delay differential equation (SDDE). Since self-regenerative chatter is typically described by delay equations, the number of studies on stochastic machining dynamics remains small, particularly in comparison to its deterministic counterpart. We note here that in addition to machining dynamics [3,4], SDDEs arise in many applications such as chemical kinetics [6] and genetic networks [7]. Therefore, developing or extending analytical and numerical tools for their analysis continues to be an active and important area of research.

For a limited number of SDDEs, stochastic calculus can be used to study the stability of the first and second moments [8]. If the delay is small, then the SDDE can be approximated using a stochastic differential equation without the delay term [9]. An extension of the semi-discretization method for studying the moment stability of linear SDDEs with delays appearing in the drift term only was described in Ref. [10]. Another method to investigate the stability of this class of equations uses Lyapunov approach [11]. However, for the general case of SDDEs numerical simulation remains the most viable method of analysis.

Euler-Maryuama and Milstein simulation methods were extended to stochastic differential equations in [12–15] and [16], respectively. Numerical simulation provides a tool for gener-

*Address all correspondence to this author.

ating path-wise solutions that can be easier to investigate than the original SDDE. For example, instead of directly studying the mean square (or more generally, the p^{th} mean) stability of the SDDE, which might be difficult or impossible, the paths generated by numerical simulation can be used [17–19]. The result of the numerical simulation is a time series or dataset that contains information about the system dynamics. Developing data analysis tools for these datasets has two benefits: 1) it provides a benchmark for testing new methods for the analysis of SDDE, and 2) the same tools can be used to analyze data from real-world applications, e.g., machining dynamics.

Some of the data analysis methods for non-delayed stochastic equations include principal component analysis [20, 21], multi-dimensional scaling [22], local linear embedding [23], Laplacian eigenmaps [24], Hessian eigenmaps [25], local tangent space alignment [26], and diffusion maps [27–29]. The first step in many of these methods is to obtain a lower-dimensional representation of the underlying high-dimensional manifold. The hope is that the simplified representation captures the main features of the underlying dynamics. One of the key assumptions in many of the prominent data analysis methods for dynamical systems, e.g., diffusion maps, is that the underlying dynamics is Markovian. This precludes them from being used to study SDDEs which are non-Markovian.

In this paper we explore data analysis tools for studying the stability of a stochastic model for turning using topological data analysis. These tools are applicable to datasets arising from both experiments as well as simulations of dynamical systems. Specifically, we will use persistent homology to automatically detect when changes in the system behavior indicative of chatter occur near the stability boundary of the linearized, noise-free model. In contrast to other data analysis tools, persistent homology does not require the system to be Markovian and it does not attempt to obtain a lower dimensional representation of a data set, but rather a low-dimensional descriptor which is easy to understand and which can be used to find quantities of interest.

We demonstrate the main concepts using a second order nonlinear stochastic delay equation with multiplicative noise that models a single degree of freedom turning process. The stochastic component is introduced using a stochastic cutting force coefficient where the source of stochasticity can be the variation in the temperature, shear angle, or workpiece material properties. In particular, we study the model SDDE in a region near the the stability boundary of the corresponding linearized, noise-free model and use Euler-Maruyama method to simulate the SDDE. We show that as the value of the delay is varied persistent homology can be used to detect the change of the response from a steady state equilibrium to a periodic orbit indicating the loss of stability through a Hopf bifurcation.

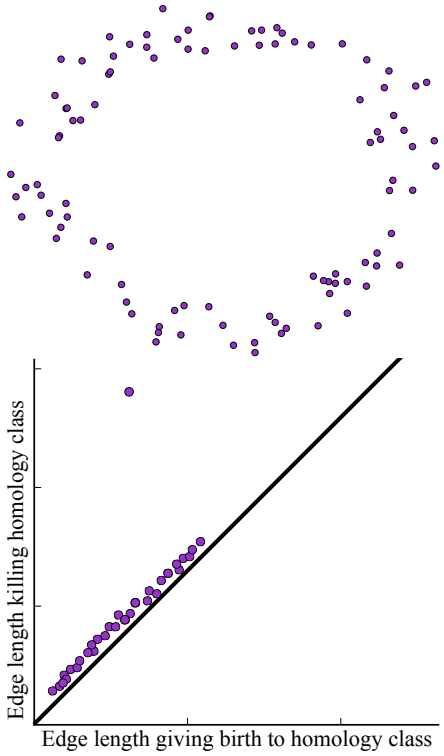

FIGURE 1. A point cloud and its persistence diagram. The circular structure of the point cloud is reflected in the single point far from the diagonal in the persistence diagram. The distance from this point to the diagonal can be used to quantify the circular structure.

PERSISTENT HOMOLOGY

Persistent homology is a powerful tool arising in the context of Topological Data Analysis (TDA). It has found success in applications to many diverse fields such as neuroscience [30], medicine [31], sensor networks [32,33], and image analysis [34]. We begin with an informal introduction to the subject, and direct the reader to [35, 36] for a full introduction to classical homology and to [37] for an introduction to persistence. Suppose we are given a point cloud drawn from a manifold and want to understand something about the underlying structure of the manifold. To do this, we consider expanding discs centered at each point. We can then study the structure of the union of these discs for a changing radius. In the example of Fig. 1, we see that at a very small radius, we have merely a set of disconnected components. At a slightly larger radius, these discs start to intersect, possibly forming small circular structures which fill in at a slightly larger radius. What is very interesting is that at a relatively small radius, we form a circular structure around the full shape, but this takes a much longer time before it fills in.

In particular, given a set of points $\chi \subset \mathbb{R}^n$, we approximate the structure of the union of discs by a Rips complex, $\mathscr{R}_r$. This is a simplicial complex which consists of a vertex v_i associated

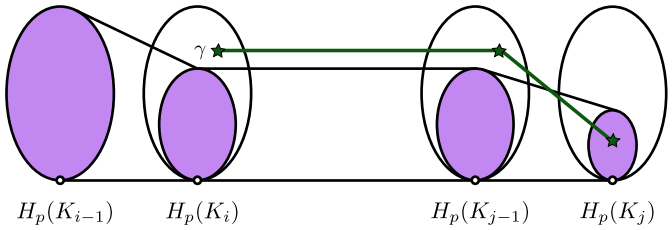

FIGURE 2. A schematic for understanding the birth and death of a persistent homology class. Classes are born if they do not appear in the image of the previous homology group under the maps induced by the filtration, and die when they merge with this image.

to each point $x_i \in \chi$, and has an edge (v_i, v_j) any time the corresponding points are within distance r of each other, $\|x_i - x_j\| \leq r$. Then higher dimensional simplices are added whenever possible; that is, the simplex σ is in $\mathscr{R}_r$ iff $\|x_i - x_j\| \leq r$ for all $v_i, v_j \in \sigma$. Notice that since $\mathscr{R}_r \subset \mathscr{R}_s$ for $r < s$, we have a filtration $\{\mathscr{R}_r\}_{r>0}$.

Let $H_p(\mathscr{R}_r)$ be the p-dimensional homology with $\mathbb{Z}_2$ coefficients. The inclusion $f : \mathscr{R}_r \hookrightarrow \mathscr{R}_s$ induces a map on homology, $f_*^{r,s} : H_p(\mathscr{R}_r) \to H_p(\mathscr{R}_s)$. A value r is called a homological critical value if for all sufficiently small $\delta > 0$, $f_*^{r-\delta,r} : H_p(\mathscr{R}_{r-\delta}) \to H_p(\mathscr{R}_r)$ is an isomorphism. Because we are interested in a finite point cloud χ, there are finitely many homological critical values; call them $r_1, \cdots, r_n$. Note that these radii are a subset of the set of pairwise distances between the points. For simplicity, we will replace $\mathscr{R}_{r_i}$ with K_i and $f_*^{r_i,r_j}$ with $f_*^{i,j}$.

A class γ is said to be born at r_i if $\gamma \in H_p(K_i)$ and it is not in the image of $f_*^{i-1,i} : H_p(K_{i-1}) \to H_p(K_i)$. This same class dies at r_j if it merges with the image of $H_p(K_{i-1})$ when entering $H_p(K_j)$; that is, if $f_*^{i,j-1}(\gamma)$ is not in $f_*^{i-1,j-1}(H_p(K_{i-1}))$ but $f_*^{i,j}(\gamma)$ is in $f_*^{i-1,j}(H_p(K_{i-1}))$. The persistence of the class is its lifetime, $r_j - r_i$. See Fig. 2.

To visualize this information, each class γ which is born at r_i and dies at r_j has a point drawn at (r_i, r_j) in what is called a persistence diagram. Classes which have small persistence show up as points close to the diagonal; classes which have large persistence appear as points far from the diagonal. In this way, we have a visual representation of the difference between classes which live a long time (and could be considered important), and the points representing short lived classes (and are often assumed to be noise).

The Delay Embedding

Since its introduction in 2000 [38], persistence has found many applications. Most recently, a great deal of work has looked at using persistence for signal analysis [39–42]. The idea behind this method is to use the Takens embedding, also known as the sliding window embedding, to turn a signal $X(t)$ into a point cloud in high dimensional space and analyze this point cloud using persistence.

The delay embedding is a standard tool for time series analysis [43]. Given a time series $X(t)$, which in practice is a set of samples $s_n = X(t_n)$, fix a delay $\eta > 0$ and chose a dimension $m \in \mathbb{Z}_{>0}$ in which to embed the data. Then the delay embedding is a lift of the time series to the map to $\mathbb{R}^m$

$$\psi_\eta^m : t \longmapsto (X(t), X(t+\eta), \cdots, X(t+(m-1)\eta)).$$

Through an important theorem of Takens [44], we are justified in using the term "embedding" since, under the correct parameter choices, this mapping preserves the structure of the underlying manifold and the dynamics of the system.

Theorem 1 (Takens Theorem). *Let M be a compact manifold of dimension m. For pairs (φ, y), $\varphi : M \to M$ a smooth diffeomorphism and $y : M \to \mathbb{R}$ a smooth function, it is a generic property that the map $\Phi_{\varphi,y} : M \to \mathbb{R}^{2m+1}$ given by*

$$\Phi_{\varphi,y}(x) = (y(x), y(\varphi(x)), \cdots, y(\varphi^{2m}(x)))$$

is an embedding.

Of course, this embedding is sensitive to the choices of the parameters m and η. A choice of m which is too low means that the structure of the embedding will not accurately reflect the dynamics; a high choice of m increases computation time due to the curse of dimensionality. A low choice of η means that the data will be overly correlated and the data will cluster around the diagonal in $\mathbb{R}^m$, yielding no information. On the other hand, a high choice of η gives an embedding which will be too spread out to say anything useful.

Luckily, methods exist which can help to intelligently choose the parameters. For the purposes of this paper, we are interested in 1-dimensional structure. Since Taken's theorem implies that 1-dimensional structure will be visible in 3-dimensional space, we have chosen $m = 3$.

The choice of the η comes from the autocorrelation function. First, given samples $(X(t_1), \cdots, X(t_N))$ for evenly spaced t_i, approximate the mean and variance of the underlying distribution using the observed values,

$$\hat{\mu} = \frac{1}{N}\sum_{n=1}^{N} X(t_i), \qquad \hat{\sigma}^2 = \frac{1}{N-1}\sum_{n=1}^{N} (X(t_n) - \hat{\mu})^2.$$

Then the autocorrelation at lag η where η is a multiple of $t_i - t_{i-1}$ and $\eta \ll (t_N - t_1)$ is given by

$$c(\eta) = \frac{1}{\hat{\sigma}^2}\left\langle (X(t_i) - \hat{\mu})(X(t_i - \eta) - \hat{\mu}) \right\rangle = \frac{\langle X(t_i)X(t_i - \eta)\rangle - \hat{\mu}^2}{\hat{\sigma}^2}.$$

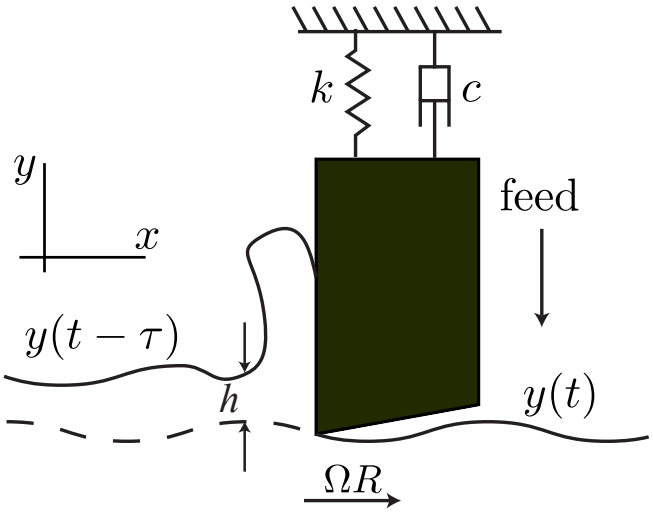

FIGURE 3. The turning process under study in this paper. The tool is compliant in x while the workpiece is assumed rigid.

The function $c(\eta)$ gives information about how the points are distributed at the choice of lag. If they cluster around the diagonals $X(t_i) = X(t_i - \eta)$ or $X(t_i) = -X(t_i - \eta)$, the autocorrelation function will be positive or negative, respectively. If, however, the points are evenly spread out, $c(\eta) = 0$. Thus, we can choose η to be the first zero of the autocorrelation function.

MATHEMATICAL MODEL

We assume that the workpiece is rigid and that the cutting tool is flexible along the y direction as shown in Fig. 3. The equation of motion for this single degree of freedom system can therefore be written as

$$\ddot{y} + 2\zeta\omega\dot{y} + \omega^2 y = \frac{F}{m} \tag{1}$$

where ζ is the damping ratio, ω is the natural frequency of the tool, m is the modal mass, and F is the cutting force. We use the power model for the cutting force which is assumed to depend on the uncut chip thickness according to

$$F = K_y w h^{\alpha} \tag{2}$$

where K_y is the mechanistic cutting coefficient, w is the depth of cut, h is the chip thickness, and the exponent is typically chosen as $\alpha = 0.75$. Due to the compliance of the tool, the chip thickness varies dynamically in time according to

$$h = \begin{cases} h_0 + y(t-\tau) - y(t) & \text{if } y(t) - y(t-\tau) \le h_0 \\ 0 & \text{otherwise} \end{cases} \tag{3}$$

where h_0 is the nominal feed rate per revolution. To reduce the number of parameters in Eq. (1), we use the rescaling used in [45]: let $y(t) = h_0\tilde{y}(t)$ and rescale time such that $\tilde{t} = \omega t$ and $\tilde{\tau} = \omega\tau$. After dropping the tildes, the resulting equation reads

$$\begin{aligned} \ddot{y} + 2\zeta\dot{y} + y &= \frac{K_y w (2\pi R)^{\alpha-1}}{m\omega^2}\rho^{\alpha-1}(1 + y(t-\tau) - y(t))^{\alpha} \\ &= K\rho^{\alpha-1}(1 + y(t-\tau) - y(t))^{\alpha} \end{aligned} \tag{4}$$

where R is the radius of the workpiece, $\rho = h_0/(2\pi R)$, and K is the dimensionless depth of cut. Typical values for ρ in conventional turning are $\rho < 0.01$. The corresponding condition for the tool to be in contact with the workpiece is

$$y(t) - y(t-\tau) \le 1. \tag{5}$$

From Eq. (4) it can be seen that the constant steady state solution is $K\rho^{\alpha-1}$. Equation (4) along with condition (5) will be used in a simulation to generate time series for the deterministic system.

If we allow the dimensionless cutting coefficient to become a stochastic variable due to variations in the workpiece material, shear angle, or temperature effects, then we can write the stochastic cutting coefficient $\hat{K}$ as

$$\hat{K} = \bar{K} + \delta\frac{dB}{dt} \tag{6}$$

where $\bar{K}$ is the average or nominal value of the cutting coefficient, δ is the diffusion coefficient while B is a standard Brownian motion. Using the above definition, the stochastic delay differential equation describing the tool oscillations reads

$$\begin{aligned} d\dot{Y} = &\left(-2\zeta\dot{Y} - Y + \bar{K}\rho^{\alpha-1}(1 + Y(t-\tau) - Y(t))^{\alpha}\right)dt \\ &+ \delta\left(\rho^{\alpha-1}(1 + Y(t-\tau) - Y(t))^{\alpha}\right)dB. \end{aligned} \tag{7}$$

Where Eq. (7) is interpreted in the Itô sense [46].

Let $h = (1 + Y(t-\tau) - Y(t))$, then we can write Eq. (7) as a pair of first order equations for the position and velocity of the tool according to

$$\begin{aligned} dY &= d\dot{Y}dt, \\ d\dot{Y} &= \left(-2\zeta\dot{Y} - Y + \bar{K}\rho^{\alpha-1}h^{\alpha}\right)dt + \delta\left(\rho^{\alpha-1}h^{\alpha}\right)dB. \end{aligned} \tag{8}$$

Equation (8) is nonlinear stochastic delay differential equation with multiplicative noise and it will be used in an Euler-Maruyama simulation to generate time series that will be studied using persistence homology.

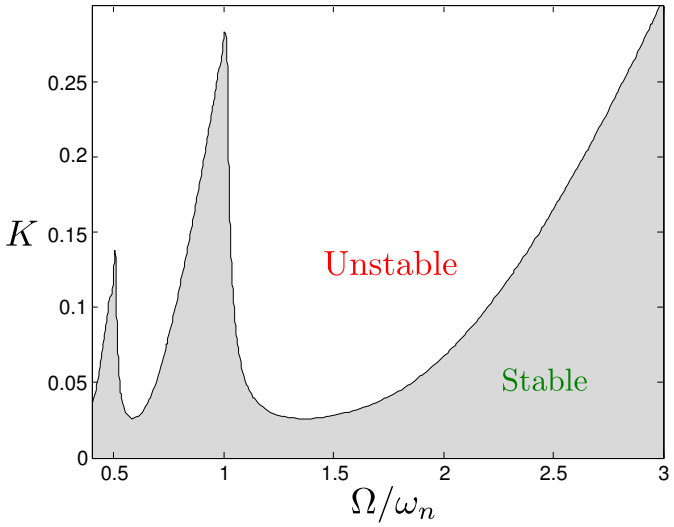

FIGURE 4. The stability diagram for Eq. (9) using $\zeta = 0.03$, $\rho = 0.01$, and $\alpha = 0.75$.

LINEARIZED STABILITY ANALYSIS

Linearizing Eq. (4) around the steady state solution ,we get the linear delay differential equation

$$\ddot{\xi} + 2\zeta\dot{\xi} + y = \alpha K \rho^{\alpha-1}(\xi(t-\tau) - \xi(t)) \tag{9}$$

Equation (4) describes the oscillations of the tool assuming a deterministic model and it will be used for obtaining the stability of the linearized deterministic system.

Equation (9) is linear autonomous delay differential equation whose stability can be studied using several methods in the literature, e.g., zero-order approximation [47], semi-discretization [48], Chebyshev collocation [49], or spectral element method [50]. In this study we use the spectral element method with one temporal element, a polynomial of degree 12, and a 100×100 grid in the $(\Omega/\omega_n, K)$ plane. We suppress the details of the spectral element method and instead refer the reader to [50] for a more thorough description.

The resulting stability diagram is shown in Fig. 4. Shaded regions are stable while unshaded regions are unstable. The results are in agreement with the semi-discretization solution in [45].

NUMERICAL SIMULATION

Two different simulations were used: an explicit Runge-Kutta triple via Matlab's DDE23 command for the deterministic case in (4), and an Euler-Maruyama simulation for the stochastic system (8). Each of these two simulations is discussed in more detail within the following sections. The system parameters that were used in the simulations are identical to the ones used for the stability analysis in Fig. 4. The simulation was performed over the $(\Omega/\omega_n, K)$ region near the deterministic stability boundary as shown in Fig. 6. The simulations were initialized by setting the history function equal to the steady state solution $K\rho^{\alpha-1}$ for $t \in [-\tau, 0]$ and a small perturbation (we chose 0.01) was introduced at $t = 0$ as shown in Fig. 5b. The information obtained from the simulation was then used to update the profile of the workpiece in subsequent revolutions as shown in Fig. 5c.

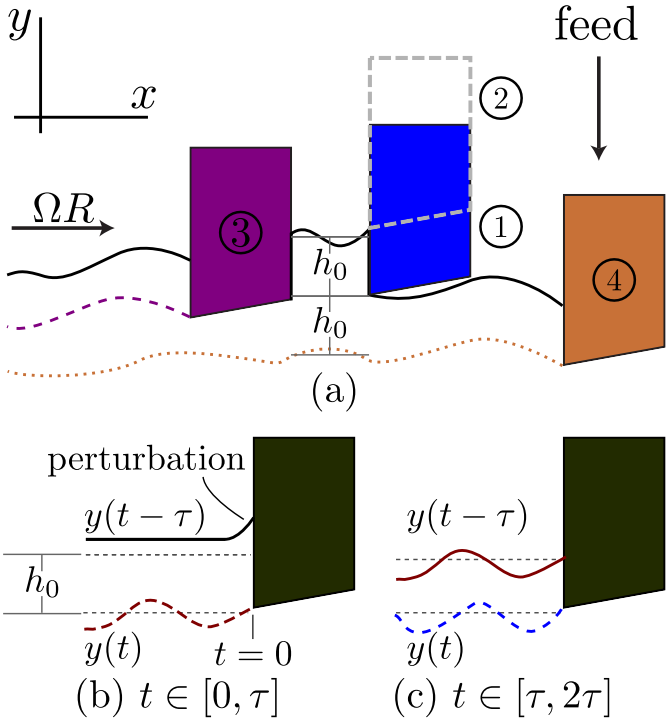

FIGURE 5. Snapshots of the turning process. (a) The change in the surface profile due to loss of contact between position 2 and 3 modifies the uncut chip thickness that the tool sees in the following revolution (position 4). (b) The history function during the first revolution is chosen to be the equilibrium solution with a small perturbation at $t = 0$. (c) For subsequent revolutions (the second workpiece revolution is shown here), the surface profile is updated according to the tool oscillations in the previous revolution.

Deterministic case simulation

Equation (4) was simulated using Matlab's DDE23 function. The 'Events' option was used to monitor condition (5) and it terminated the simulation as soon as the tool lost contact with workpiece. The system was simulated over $t \in [0, 200]$ but the time series corresponding to unstable cuts were shorter because of the early termination of the simulation due to the tool exiting the cut.

Stochastic case simulation

Equation (7) was simulated using the Euler-Maryuama method, described in [12], to generate the necessary datasets. The Brownian path was created using Matlab and the approach described in [51]. The equation was simulated over $[0, M \times \tau]$ where we chose $M = 2^5$. We used two values for the noise intensity δ in Eq. (8): $\delta = 0.01$ and $\delta = 0.10$. The number of points for generating the Brownian path is $N = M \times 2^{14}$. The time steps for the Brownian path and for the Euler-Maryama simulation are dt and Δt, respectively. In this study, we set $\Delta t = dt = t_f/N$. This choice of the simulation parameters enabled mapping the term $Y(t-\tau)$ exactly onto both a point on the Brownian path and a point that was simulated previously thus eliminating the need for estimating intermediate values. The time for each spindle revolution, which is equal to the time delay, is an integer multiple of the simulation time step according to

$$\tau = \frac{N}{M}\Delta t. \tag{10}$$

This means that the profile left behind in any workpiece revolution is discretized using N/M points.

Condition (5) was monitored during the stochastic simulation; however, in contrast to the deterministic case, the simulation was not terminated when the tool left the workpiece. Instead, the forcing term was turned off and the tool was subject to free oscillations. This means that it was possible for the tool to go in and out of the cut multiple times during the duration of the simulation. Figure 5 shows four snapshots of the tool related to the loss of contact. Snapshots 1 and 2 show the tool right before and right after it lost contact with the workpiece. Between snapshots 2 and 3 the tool experiences free damped oscillations outside of the cut until it returns to the cut in snapshot 3. Consequently, during the next revolution the tool encounters the surface that was not cut due to the loss of contact as shown by snapshot 4. The code kept track of all the loss of contact events and updated the N/M surface profile representation points left behind accordingly.

PERSISTENCE COMPUTATION

We next analyzed the time series generated by the numerical simulation using persistent homology. The time series $X_{\omega,K}(t)$ was given as a series of samples $s_n = X_{\omega,K}(t_n)$ for $t_n \in [0,T]$. First, for each simulation we limited the domain of interest to $t \in [100-T, T]$. The dimension m of Euclidean space in which to embed the point cloud was chosen to be 3. The parameter η was chosen for each simulation using the first zero of the autocorrelation function. Then the point cloud consisted of points

$$\psi^3_\eta(t_n) = (X_{\omega,K}(t_n), X_{\omega,K}(t_n+\eta), X_{\omega,K}(t_n+2\eta))$$

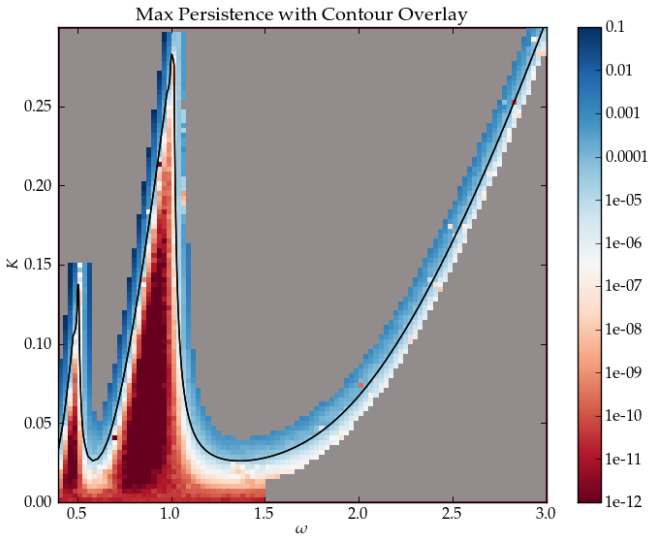

FIGURE 6. The maximum persistence for the simulations with no added noise is shown by log-scaled color values. The line drawn is the stability boundary from Fig. 4. Note that the change in maximum persistence values corresponds to the change from the stable to the unstable regions.

for $t_n \in [T-100, T-2\eta]$. When necessary for speeding up the computation, the point cloud was sparsified before computing persistence by keeping every i^{th} point in order to have between 200 and 500 points. Persistence was computed on this point cloud using the M12 package [52], and the maximum persistence of all points in the 1-dimensional persistence diagram was saved.

RESULTS AND CONCLUSIONS

For the case of noise-free turning described by Eq. (4), figure 6 shows that the persistence diagram captured the stability behavior. This can be seen by comparing Figs. 6 and 4 where the latter was obtained using the spectral element approach. Figure 6 shows that the maximum persistence switches from almost zero below the stability boundary to a much higher value across the unstable region of the boundary. Therefore, even though the simulation was terminated as soon as the tool jumped out of the cut, persistence was still able to detect the onset of chatter associated with going from a stable equilibrium to an unstable oscillatory behavior via Hopf bifurcation.

Figure 7 shows the persistence diagrams associated with the Euler-Maruyama simulation of Eq. (8) at two different noise intensities: $\delta = 0.01$ and $\delta = 0.1$. For the low noise level, Fig. 7 shows a stability behavior similar to the noise-free case in Fig. 6 near the first and second lobes. However, we observe distinct differences between the case of high and low noise near these two lobes. Specifically, whereas maximum persistence is higher to

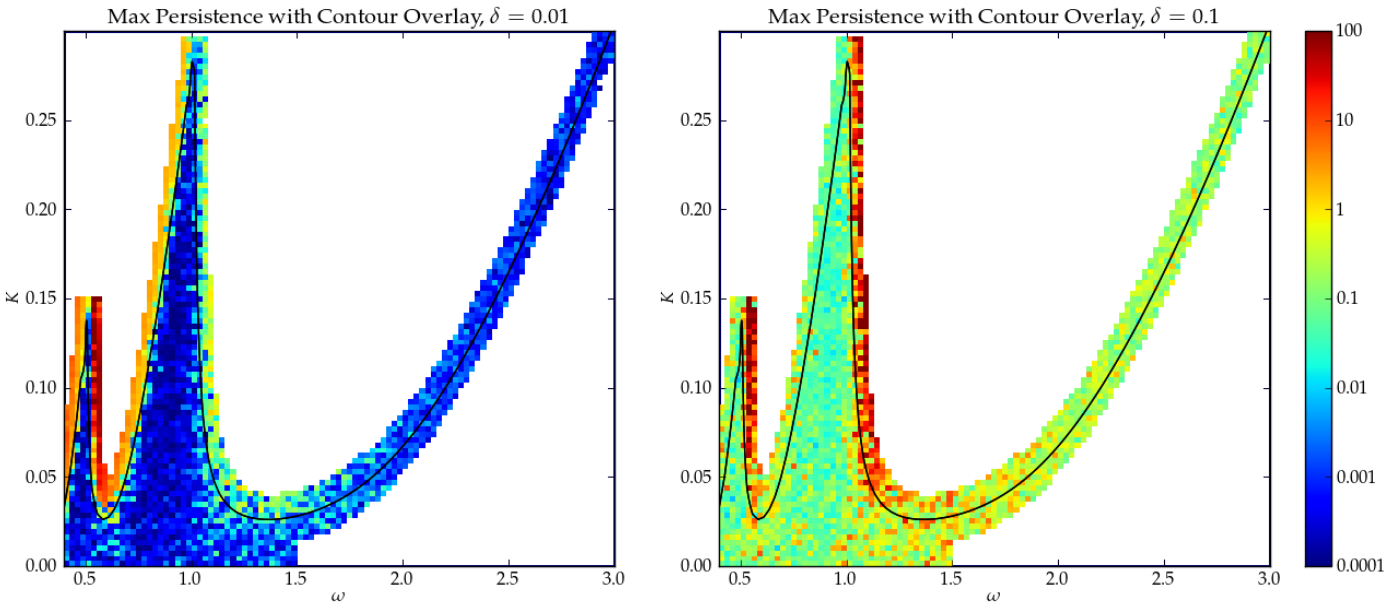

FIGURE 7. The maximum persistence for the simulations with noise $\delta = 0.01$ is shown at left and with noise $\delta = 0.1$ is shown at right. The value of the maximum persistence is denoted by log-scaled color values. The line drawn is the stability boundary from Fig. 4. Increasing the noise intensity changes the region of high persistence from the left side of the first two lobes to the right side. Further, noise seems to have a stabilizing effect in comparison to the noise-free case in Fig. 6.

the left of the first two lobes for $\delta = 0.01$, the highest values of maximum persistence occur to the right of the lobes for $\delta = 0.1$. This suggests that machining near the right side of the stability lobes is more prone to experiencing abrupt transition to chatter at higher levels of noise.

Another observation is that the maximum persistence near the third stability boundary for both noise levels does not experience the large increase across the deterministic stability boundary shown in Fig. 6 for the noise-free case. This suggests that in this region of the $(\Omega/\omega_n, K)$ parameter space, noise seems to have a stabilizing effect on the system in comparison to the deterministic case. The new instability boundaries for the noisy model are beyond the considered band near the deterministic stability boundary. The authors are currently expanding the simulated region of the parameter space to capture the new stability boundaries for the noisy models.

The results of this study show that persistent homology capture the change in the qualitative behavior of the system associated with a bifurcation. In the context of machining dynamics, this means that persistence can be used to detect the onset of chatter. Although the datasets that we investigated were generated using simulation, the developed method is equally applicable to experimental data. The analysis showed that increasing the noise intensity changes the side of the stability lobes that is likely to experience more abrupt transitions to chatter. Further, we found that noise has as a stabilizing effect near the third lobe. The reason for these changes in the stability behavior is a topic of our ongoing research.

ACKNOWLEDGMENT

The authors thank Jose Perea for extremely helpful discussions. The work described in this article is a result of a collaboration made possible by the Institute for Mathematics and Its Applications. It was carried out while EAM was a postdoctoral fellow at the IMA during the annual program on Scientific and Engineering Applications of Algebraic Topology. FAK gratefully acknowledges the support and hospitality provided by the IMA during his visit which took place in February 2014.

REFERENCES

[1] Quintana, G., and Ciurana, J., 2011. "Chatter in machining processes: A review". *International Journal of Machine Tools and Manufacture,* ***51***(5), pp. 363–376.

[2] Kuske, R., 2006. "Multiple-scales approximation of a coherence resonance route to chatter". *Computing in Science Engineering,* ***8***(3), pp. 35–43.

[3] Buckwar, E., Kuske, R., L'Esperance, B., and Soo, T., 2006. "Noise-sensitivity in machine tool vibrations". *International Journal of Bifurcation and Chaos,* ***16***(08), pp. 2407–2416.

[4] Klamecki, B., 2004. "Enhancement of the low-level components of milling vibration signals by stochastic resonance". *Proceedings of the Institution of Mechanical Engineers, Part E: Journal of Process Mechanical Engineering,* ***218***(1), pp. 33–41.

[5] Yilmaz, A., AL-Regib, E., and Ni, J., 2002. "Machine tool chatter suppression by multi-level random spindle speed variation". *Journal of Manufacturing Science and Engineering,* ***124***(2), pp. 208–216.

[6] Barrio, M., Burrage, K., Leier, A., and Tian, T., 2006. "Oscillatory regulation of hes1: Discrete stochastic delay modelling and simulation". *PLoS Comput Biol,* ***2***(9), 09, p. e117.

[7] Tian, T., Burrage, K., Burrage, P. M., and Carletti, M., 2007. "Stochastic delay differential equations for genetic regulatory networks". *Journal of Computational and Applied Mathematics,* ***205***(2), pp. 696 – 707. Special issue on evolutionary problems.

[8] Mackey, M. C., and Nechaeva, I. G., 1995. "Solution moment stability in stochastic differential delay equations". *Phys. Rev. E,* ***52***(4), Oct, pp. 3366–3376.

[9] Guillouzic, S., L'Heureux, I., and Longtin, A., 1999. "Small delay approximation of stochastic delay differential equations". *Phys. Rev. E,* ***59***, Apr, pp. 3970–3982.

[10] Elbeyli, O., Sun, J., and Unal, G., 2005. "A semi-discretization method for delayed stochastic systems". *Communications in Nonlinear Science and Numerical Simulation,* ***10***(1), pp. 85–94.

[11] Frank, T. D., and Beek, P. J., 2001. "Stationary solutions of linear stochastic delay differential equations: Applications to biological systems". *Phys. Rev. E,* ***64***, Jul, p. 021917.

[12] Buckwar, E., 2000. "Introduction to the numerical analysis of stochastic delay differential equations". *Journal of Computational and Applied Mathematics,* ***125***(1-2), pp. 297 – 307. Numerical Analysis 2000. Vol. VI: Ordinary Differential Equations and Integral Equations.

[13] Mao, X., and Sabanis, S., 2003. "Numerical solutions of stochastic differential delay equations under local lipschitz condition". *Journal of Computational and Applied Mathematics,* ***151***(1), pp. 215 – 227.

[14] Yuan, C., and Glover, W., 2006. "Approximate solutions of stochastic differential delay equations with markovian switching". *Journal of Computational and Applied Mathematics,* ***194***(2), pp. 207 – 226.

[15] Buckwar, E., and Winkler, R., 2007. "Multi-step maruyama methods for stochastic delay differential equations". *Stochastic Analysis and Applications,* ***25***(5), pp. 933–959.

[16] Hu, Y., Mohammed, S.-E. A., and Yan, F., 2004. "Discrete-time approximations of stochastic delay equations: The milstein scheme". *Annals of Probability,* ***32***(1A), pp. 265–314.

[17] Baker, C. T. H., and Buckwar, E., 2005. "Exponential stability in p-th mean of solutions, and of convergent euler-type solutions, of stochastic delay differential equations". *J. Comput. Appl. Math.,* ***184***(2), Dec., pp. 404–427.

[18] Luo, J., 2007. "A note on exponential stability in pth mean of solutions of stochastic delay differential equations". *Journal of Computational and Applied Mathematics,* ***198***(1), pp. 143 – 148.

[19] Mao, X., 2007. "Exponential stability of equidistant euler-maruyama approximations of stochastic differential delay equations". *Journal of Computational and Applied Mathematics,* ***200***(1), pp. 297 – 316.

[20] Jolliffe, I., 2005. *Principal Component Analysis*. John Wiley & Sons, Ltd.

[21] Abdi, H., and Williams, L. J., 2010. "Principal component analysis". *Wiley Interdisciplinary Reviews: Computational Statistics,* ***2***(4), pp. 433–459.

[22] Borg, I., and Groenen, P. J. F., 2005. *Modern Multidimensional Scaling: Theory and Applications*. Springer.

[23] Roweis, S., and Saul, L., 2000. "Nonlinear dimensionality reduction by locally linear embedding". *Science,* ***290***(5500), p. 23232326.

[24] Belkin, M., and Niyogi, P., 2003. "Laplacian eigenmaps for dimensionality reduction and data representation". *Neural Computation,* ***15***(6), pp. 1373–1396.

[25] Donoho, D. L., and Grimes, C., 2003. "Hessian eigenmaps: Locally linear embedding techniques for high-dimensional data". *Proceedings of the National Academy of Sciences,* ***100***(10), pp. 5591–5596.

[26] Zhang, Z., and Zha, H., 2002. "Principal manifolds and nonlinear dimension reduction via local tangent space alignment". *SIAM Journal of Scientific Computing,* ***26***, pp. 313–338.

[27] Coifman, R. R., and Lafon, S., 2006. "Diffusion maps". *Applied and Computational Harmonic Analysis,* ***21***(1), pp. 5 – 30. Special Issue: Diffusion Maps and Wavelets.

[28] Nadler, B., Lafon, S., Coifman, R. R., and Kevrekidis, I. G., 2006. "Diffusion maps, spectral clustering and reaction coordinates of dynamical systems". *Applied and Computational Harmonic Analysis,* ***21***(1), pp. 113 – 127. Special Issue: Diffusion Maps and Wavelets.

[29] Singer, A., and Coifman, R. R., 2008. "Non-linear independent component analysis with diffusion maps". *Applied and Computational Harmonic Analysis,* ***25***(2), pp. 226 – 239.

[30] Brown, J., and Gedeon, T., 2012. "Structure of the afferent terminals in terminal ganglion of a cricket and persistent homology". *PLoS ONE,* ***7***(5), 05, p. e37278.

[31] Nicolau, M., Levine, A. J., and Carlsson, G., 2011. "Topology based data analysis identifies a subgroup of breast cancers with a unique mutational profile and excellent survival". *Proceedings of the National Academy of Sciences,*

108(17), pp. 7265–7270.

[32] de Silva, V., and Ghrist, R., 2007. "Coverage in sensor networks via persistent homology". *Algebraic & Geometric Topology,* ***7***, Apr., pp. 339–358.

[33] Munch, E., Shapiro, M., and Harer, J., 2012. "Failure filtrations for fenced sensor networks". *The International Journal of Robotics Research,* ***31***(9), pp. 1044–1056.

[34] Carlsson, G., Ishkhanov, T., de Silva, V., and Zomorodian, A., 2008. "On the local behavior of spaces of natural images". *International Journal of Computer Vision,* ***76***, pp. 1–12. 10.1007/s11263-007-0056-x.

[35] Munkres, J. R., 1993. *Elements of Algebraic Topology*. Addison Wesley.

[36] Hatcher, A., 2002. *Algebraic Topology*. Cambridge University Press.

[37] Edelsbrunner, H., and Harer, J., 2010. *Computational Topology: An Introduction*. American Mathematical Society.

[38] Edelsbrunner, H., Letscher, D., and Zomorodian, A., 2000. "Topological persistence and simplification". In Foundations of Computer Science, 2000. Proceedings. 41st Annual Symposium on, pp. 454 –463.

[39] Perea, J. A., and Harer, J., 2013. "Sliding windows and persistence: An application of topological methods to signal analysis". *arXiv:1307.6188*.

[40] Berwald, J., Gidea, M., and Vejdemo-Johansson, M., 2013. "Automatic recognition and tagging of topologically different regimes in dynamical systems". *arXiv:1312.2482*.

[41] de Silva, V., Skraba, P., and Vejdemo-Johansson, M., 2012. "Topological analysis of recurrent systems". In NIPS 2012 Workshop on Algebraic Topology and Machine Learning.

[42] Emrani, S., Gentimis, T., and Krim, H., 2014. "Persistent homology of delay embeddings and its application to wheeze detection". *Signal Processing Letters, IEEE,* ***21***(4), April, pp. 459–463.

[43] Kantz, H., and Schreiber, T., 2004. *Nonlinear Time Series Analysis*. Cambridge University Press.

[44] Takens, F., 1981. "Detecting strange attractors in turbulence". In *Dynamical Systems and Turbulence, Warwick 1980*, D. Rand and L.-S. Young, eds., Vol. 898 of *Lecture Notes in Mathematics*. Springer Berlin Heidelberg, pp. 366–381.

[45] Insperger, T., Barton, D. A., and Stepan, G., 2008. "Criticality of hopf bifurcation in state-dependent delay model of turning processes". *International Journal of Non-Linear Mechanics,* ***43***(2), pp. 140 – 149.

[46] Oksendal, B., 2007. *Stochastic differential equations*, 6th ed. Springer.

[47] Altintaş, Y., and Budak, E., 1995. "Analytical prediction of stability lobes in milling". *CIRP Annals,* ***44***(1), pp. 357–362.

[48] Insperger, T., and Stépán, G., 2004. "Updated semi-discretization method for periodic delay-differential equations with discrete delay". *International Journal for Numerical Methods,* ***61***, pp. 117–141.

[49] Butcher, E. A., and Bobrenkov, O. A., 2011. "On the chebyshev spectral continuous time approximation for constant and periodic delay differential equations". *Communications in Nonlinear Science and Numerical Simulation,* ***16***(3), pp. 1541 – 1554.

[50] Khasawneh, F. A., and Mann, B. P., 2011. "A spectral element approach for the stability of delay systems". *International Journal for Numerical Methods in Engineering,* ***87***(6), pp. 566–592.

[51] Higham, D., 2001. "An algorithmic introduction to numerical simulation of stochastic differential equations". *SIAM Review,* ***43***(3), pp. 525–546.

[52] Harer, J., Slaczedek, J., and Bendich, P., 2014. "Ripscollapse: discrete morse theory and fast computation of one-dimensional persistence.". *Manuscript, Duke University*.